Bio-Design and Manufacturing (2025) 8:570–580
https://doi.org/10.1631/bdm.2500018

RESEARCH ARTICLE

Mechanical regulation and 3D bioprinting of native tissue-inspired granular composite hydrogels

Heyuan Deng[1,2,3] · **Yongcong Fang**[1,2,3,4,5] · **Zhengxun Gao**[1,2,3] · **Bingyan Wu**[1,2,3] · **Ting Zhang**[1,2,3,4] · **Zhuo Xiong**[1,2,3,5]

Received: 9 January 2025 / Accepted: 25 March 2025

Abstract

Granular composite (GC) hydrogels have attracted considerable interest in biomedical applications due to their versatile printability and exceptional mechanical properties. However, the lack of comprehensive design guidelines has limited their optimal engineering, as the factors influencing their mechanical performance and printability remain largely unexamined. In this study, we developed GC hydrogels by integrating microgels with interstitial matrices of photocrosslinkable gelatin methacrylate (GelMA). We utilized confocal microscopy and nanoindentation analyses to investigate the spatial distribution and mechanical behavior of these hydrogels. Our findings indicate that the mechanical and rheological properties of GC hydrogels can be precisely tailored by adjusting the volume fraction and size of the microgels. Furthermore, hydrogen bonds were identified as significant contributors to compressive performance, although they had minimal effect on cyclic mechanical behavior. Compared to bulk GelMA hydrogels, GC hydrogels demonstrated enhanced printability and remarkable superelasticity. As a proof of concept, we illustrated their dual printability in embedded printing to create prosthetic liver models for preoperative planning. This study provides valuable insights into the design and optimization of GC hydrogels for advanced biomedical applications.

✉ Yongcong Fang
fangyc@tsinghua.edu.cn

✉ Ting Zhang
t-zhang@mail.tsinghua.edu.cn

✉ Zhuo Xiong
xiongzhuo@tsinghua.edu.cn

[1] Biomanufacturing Center, Department of Mechanical Engineering, Tsinghua University, Beijing 100084, China

[2] Biomanufacturing and Rapid Forming Technology Key Laboratory of Beijing, Beijing 100084, China

[3] “Biomanufacturing and Engineering Living Systems” Innovation International Talents Base (111 Base), Beijing 100084, China

[4] State Key Laboratory of Tribology in Advanced Equipment, Tsinghua University, Beijing 100084, China

[5] State Key Laboratory of Clean and Efficient Turbomachinery Power Equipment, Department of Mechanical Engineering, Tsinghua University, Beijing 100084, China

Graphical abstract

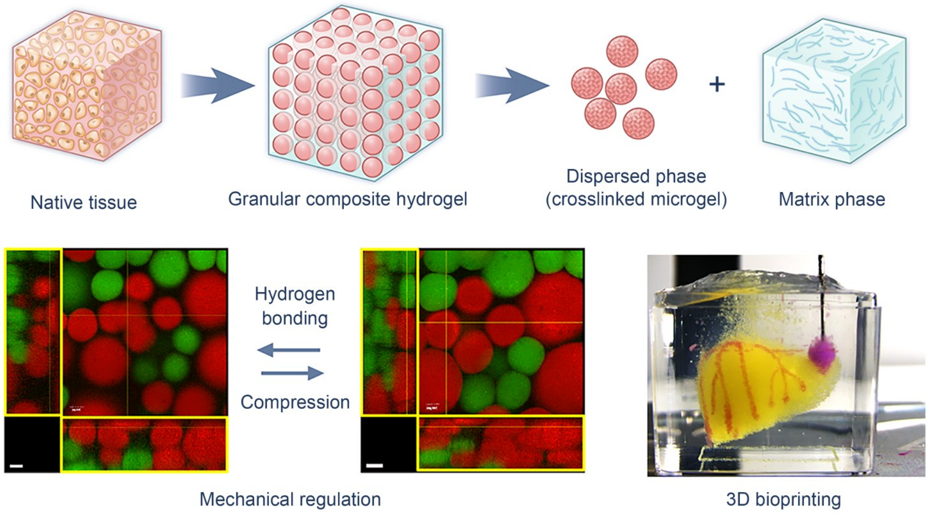

Keywords Granular composite hydrogel · 3D bioprinting · Microgel · Superelasticity · Preoperative planning

1 Introduction

Hydrogels, recognized for their high water content and biocompatibility, are seen as versatile materials for biomedical [1, 2] and tissue engineering applications [3–5]. Traditional single-component hydrogels often exhibit suboptimal mechanical properties due to their high water content, low solid-phase fraction, uneven polymer distribution, and limited energy dissipation mechanisms [6]. Advancements over the last two decades have significantly improved the mechanics of hydrogels. At the molecular level, innovative chemical strategies have introduced novel architectures, such as topological hydrogels [7–10], homogeneous four-arm gels [11, 12], and double-network hydrogels [13–16], which enhance stress distribution and energy dissipation. In addition, physical strategies, such as the incorporation of hydrogen bonds [17, 18], ionic interactions [19], and hydrophobic domains [20], further increase toughness and introduce sacrificial bonds to dissipate energy. At the macroscopic scale, innovations such as microphase-separated structures [21] have provided hydrogels with improved crack resistance, expanding their potential applications in soft robotics and flexible electronics.

Recently, granular hydrogels have attracted attention for their distinctive mechanical and rheological properties. These hydrogels are formed by compacting microgels through centrifugation or vacuum techniques, with stabilization achieved by physical/chemical crosslinking. As a result, they exhibit solid-like behavior at rest and fluid-like behavior under shear stress [22]. These characteristics make granular hydrogels suitable for applications such as bioprinting and cell culture scaffolds. Burdick pioneered their use as conductive bioinks for muscle defect repair [23]. However, the weak interactions among microgels limit the structural integrity of granular hydrogels, which constrains their broader applicability [24].

Inspired by the biphasic composition of human tissues such as adipose, our team previously developed a granular composite (GC) hydrogel that combines microgels as the dispersed (D phase) with a secondary hydrogel precursor as the interstitial matrix (M phase) (Fig. 1a) [25]. This biphasic design enhances mechanical stability and creates a heterogeneous cellular microenvironment for tissue engineering while maintaining the injectability and printability characteristics of traditional granular hydrogels. Our GC hydrogel demonstrates exceptional fatigue resistance, supports rapid cell self-assembly, and facilitates capillary formation [25, 26]. Similarly, Deo et al. developed biphasic bioinks that combine poly(ethylene glycol) (PEG)-based microgels with a gelatin methacrylate (GelMA)-nanosilicate matrix for heterogeneous tissue fabrication [27]. However, existing studies have so far primarily focused on material design, leaving an unexplored gap in understanding the mechanisms that govern the mechanical and rheological properties of GC hydrogels.

To address this gap, we systematically investigated the mechanical and rheological properties of GelMA-based GC hydrogels from macroscopic and microscopic perspectives. We adjusted the macroscopic architecture by varying the ratios and sizes of the microgels and simultaneously fine-tuning the microscopic interactions through hydrogen bonds. In addition, we successfully fabricated a vascularized liver

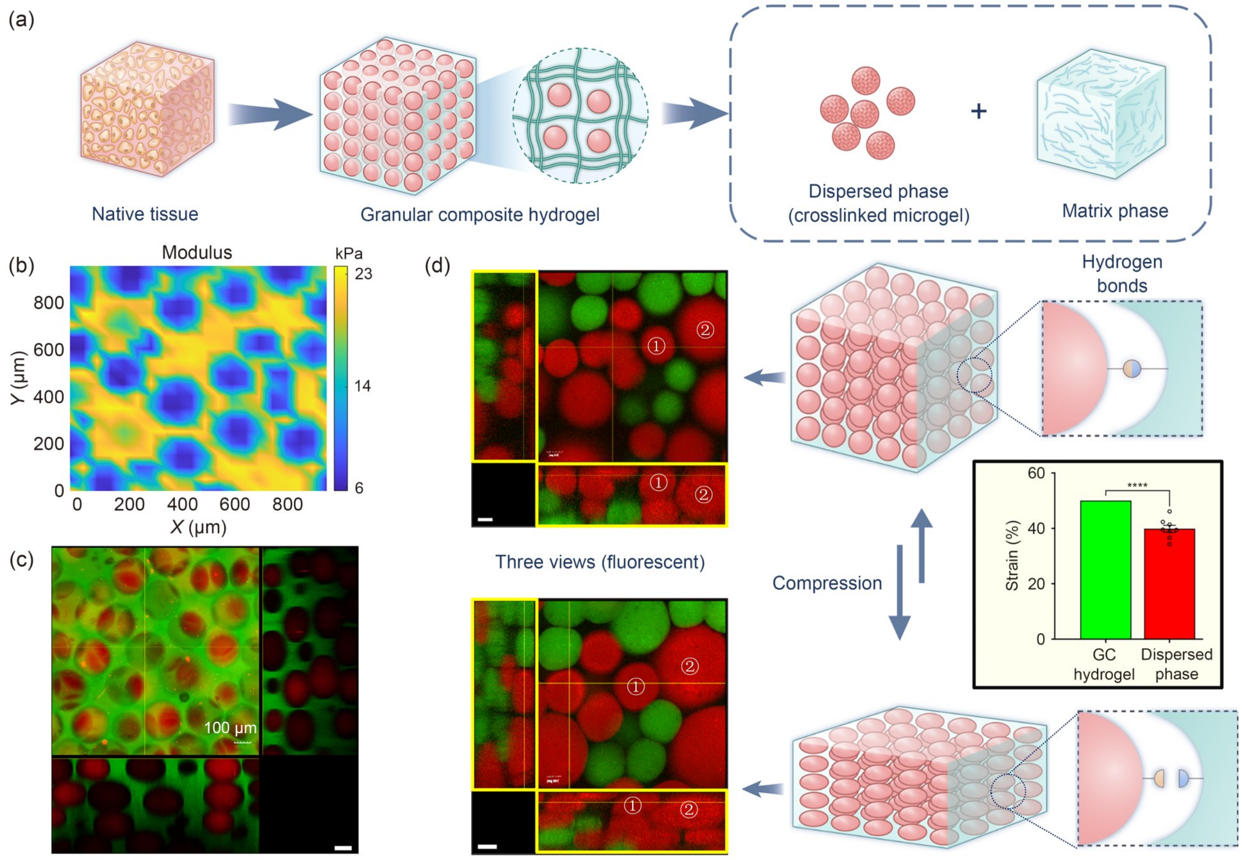

Fig. 1 Design and characterization of the GC hydrogel: (a) schematic of the design principle of the GC hydrogel inspired by native tissues; (b) nanoindentation image of the cross-section of the GC hydrogel; (c) confocal image of the GC hydrogel consisting of microgels (7.5% GelMA, highlighted in red fluorescence) and an interstitial matrix (7.5% GelMA, highlighted in green fluorescence); (d) confocal images and schematics of the GC hydrogel consisting of two types of microgels (7.5% GelMA, highlighted in red and green fluorescence) and the interstitial matrix during the compression process. Inset in (d): comparison of the deformation of the microgels and GC hydrogels during compression. Scale bars in (c, d): 100 μm. One- and two-way analysis of variance (ANOVA) were used to analyze the data. Data in (d) are expressed as mean±standard deviation (n=8). $^{****}p<0.0001$

model with embedded vascular networks and tumors to aid in preoperative surgical planning by leveraging the dual printability of the GC hydrogel. This work provides a rational framework for designing GC hydrogels with tailored properties to meet diverse needs in the biomedical field.

2 Materials and methods

2.1 Materials

GelMA hydrogels with a methacrylate substitution degree of 60% and lithium phenyl-2,4,6-trimethylbenzoylphosphinate (LAP) were obtained from TissHUe Biomedical Technology (Beijing) Co., Ltd. (China). Fluorescently labeled GelMA hydrogels (red and green) for visualization and polyethyleneglycol diacrylate (PEGDA) were sourced from EFL Inc. (China). Aristoflex alginate void chamber (AVC) was provided by Clariant Inc. (Switzerland), and urea was purchased from Greagent, Inc. (China).

2.2 Microgel generation by microfluidics

Microgels were fabricated using a polydimethylsiloxane (PDMS)-based single-channel microfluidic device. SU-8 resin molds prepared by stereolithography were used to cast PDMS (Sylgard 184; Dow Corning, USA), which was cured at 70 °C for 1 h. Inlet and outlet channels were created with a 0.75-mm biopsy punch, cleaned, and bonded to glass slides through plasma treatment. Silicone tubing was inserted into the channels. Light mineral oil (Sigma, USA) with 2% (volume fraction) Span 80 was used as the continuous phase (flow rate: 5 mL/h), and the dispersed phase consisted of a polymer precursor solution (7.5% (mass fraction) GelMA or 20% PEGDA) (flow rate: 0.75 mL/h). Droplets were crosslinked under a 405-nm visible light source (approximately 40 mW/cm^2) for 30–60 s. The resulting microgels were washed and suspended in phosphate-buffered saline (PBS) following centrifugation at 1200 r/min for 3 min to remove the oil phase and then stored for subsequent use.

2.3 Microgel generation by batch emulsion

A GelMA solution (10 mL) was added to 90 mL of light mineral oil containing 2% (volume fraction) Span 80 under continuous stirring (500 r/min) in an ice-water bath. After 20 min, the emulsion was exposed to a 405-nm light source (approximately 40 mW/cm^2) for 30–60 s to crosslink the microgels. The microgels were then washed, centrifuged to remove the oil layer, and stored in PBS for later use.

2.4 GC hydrogel preparation

Microgels suspended in PBS were centrifuged to remove excess liquid, followed by mixing with a GelMA solution. This process was repeated three times to replace the inter-microgel spaces with the GelMA phase. The resulting GC hydrogel samples were exposed to 405 nm light (approximately 20 mW/cm^2) for 30 s to crosslink. Fluorescently labeled GelMA (in red and green) was used to visualize the microgel and hydrogel phases, respectively. Confocal laser scanning microscopy with z-stack scanning was employed to observe the fluorescent GC hydrogels.

2.5 Nanoindentation

Hydrogel precursor solutions (250 μL) were confined in cylindrical molds and crosslinked under ultraviolet (UV) light for 60 s. The samples were then adhered to glass slides using high-strength adhesive and submerged in PBS throughout testing. Nanoindentation was conducted using a Chiaro nanoindenter (Optics 11, the Netherlands), equipped with a 0.45-N/m stiffness cantilever and a 49.5-μm radius spherical tip. The effective indentation modulus (E) was determined from the loading segment of the force–depth curves.

2.6 Rheological characterization

Rheological characterization was performed using an MCR301 rheometer (Anton Paar, Austria) with a 25-mm cone plate geometry and a 750-μm gap size. Shear-thinning, thermosensitive, and dynamic yielding properties were analyzed through shear rate ramps, temperature sweeps (4–37 °C), and strain sweeps (0.1%−1000%), respectively. Recovery properties were evaluated through cyclic strain tests that alternated between low (1%) and high (300%) strains.

2.7 Mechanical testing

Cylindrical samples (8 mm diameter, 5 mm height) were fabricated through casting and measured with a vernier caliper. Compression testing was performed using a Bose ElectroForce 3200 system (Bose Corp., USA) at a rate of 0.1 mm/s until failure. The elastic modulus was calculated from the stress−strain curve, and cyclic compression tests (55%−60% strain) were conducted for at least 100 cycles to evaluate performance.

2.8 Elastic modulus expression

As reported by William and David [28], the elastic modulus of composite hydrogels was bounded by E_c(u) (upper bound) and E_c(l) (lower bound), modeled using the following equations:

$$E_\mathrm{c}(\mathrm{u}) = E_\mathrm{m}V_\mathrm{m} + E_\mathrm{p}, \tag{1}$$

$$E_\mathrm{c}(\mathrm{l}) = \frac{E_\mathrm{m}E_\mathrm{p}}{V_\mathrm{m}E_\mathrm{p} + V_\mathrm{p}E_\mathrm{m}}, \tag{2}$$

where E and V represent the elastic modulus and volume fraction, respectively. Subscripts “c,” “m,” and “p” denote composite, matrix, and particle phases, respectively.

2.9 Degradation experiment

GC hydrogels were placed in 5 mL of a collagenase type II solution (1 U/mL; EFL Inc., China) and incubated at 37 °C for 2, 4, 6, and 10 h. At each time point, residual hydrogels were rinsed with ultrapure water, followed by lyophilization. Mass loss was determined by calculating the ratio of the weight loss in dried samples to the initial dry weight of the untreated hydrogels. Data were collected from three replicate samples per group at each time point.

2.10 Embedded printing

GC hydrogels were printed using an embedded printing technique. First, tissue constructs, such as brain and liver models, were printed in Aristoflex AVC. All digital models were obtained from the National Institutes of Health (NIH) 3D Print Exchange (https://3dprint.nih.gov) or created using SOLIDWORKS 2018. Each 3D model was converted to STL format and imported into SunP software for G-code generation. GC hydrogels were loaded into 3-mL syringes (BD, USA), which were then centrifuged at 1200 r/min for 30 s to remove air bubbles. The printing parameters used included a speed of 3 mm/s and an extrusion rate of 0.38 μL/s, maintained at a temperature of 24−25 °C. Following printing, the constructs were exposed to light (405 nm, approximately 20 mW/cm^2) for 30 s for crosslinking.

2.11 Sequential printing in a reversible ink template (SPIRIT)

The liver model, complete with vascular networks and a tumor, was fabricated using the SPIRIT printing technique. The liver was printed in either Aristoflex AVC or a gelatin microparticle suspension medium at a speed of 3 mm/s and an extrusion rate of 0.38 μL/s, with the temperature set to 25 °C. The internal vascular network was designed in

Geomagic Wrap, where each curvilinear line of the network was represented as piecewise linear segments to generate the G-code. For the uncrosslinked liver structure, a 7.5% gelatin ink was utilized to print the vascular network, maintaining the same speed and extrusion rate while maintaining the temperature at 24–25 °C. In addition, a 5-mm tumor sphere was printed using 7.5% GelMA. Following print completion, the construct was exposed to light (405 nm, approximately 20 mW/cm^2) for 30 s. The printed structures were then washed with PBS to eliminate the AVC suspension medium, and the gelatin microparticle suspension medium was removed by heating to 37 °C. To verify the integrity of the vascular network, the gelatin ink was dissolved at 37 °C, resulting in transparent vascular networks, which were subsequently perfused with green and purple dye-filled PBS solutions to confirm vascular continuity.

2.12 Statistical analysis

Data are presented as mean±standard deviation, derived from at least three independent samples. Statistical significance ($p < 0.05$) was determined using one- or two-way analysis of variance (ANOVA), with Tukey's honestly significant difference (HSD) test used for post hoc pairwise comparisons (GraphPad Prism 9.0 for Windows).

3 Results and discussion

3.1 Design and characterization of the GC hydrogel

In this study, we created a GC hydrogel based on GelMA, utilizing GelMA as both the microgel and the interstitial matrix. GelMA is a photocrosslinkable, gelatin-modified hydrogel that is commonly used in biomedical applications [29]. GelMA microgels were produced using microfluidics or batch emulsions and were incorporated into a GelMA precursor solution at a concentration that matched the matrix phase. The GC hydrogel was then photocrosslinked under the same conditions used for the microgel. To evaluate the microstructure and local mechanical properties, we performed nanoindentation on cross-sections of the hydrogel. The results demonstrated distinct regions of low-modulus microgels (blue in Fig. 1b) and high-modulus interstitial matrix (yellow in Fig. 1b). The reduced modulus of the microgels is likely due to swelling during the washing process. Compression simulations of the hydrogels were conducted using Abaqus, with the measured modulus values incorporated to define material properties. Figure S1a (supplementary information) shows the postcompression analysis, revealing that the interstitial matrix experienced greater strain compared to the microgels. Laser confocal microscopy further confirmed the biphasic distribution of the GC hydrogel showing red microgels surrounded by a green interstitial matrix that fills the gaps between them (Fig. 1c). In situ observations of the compression process also indicated notable differences in deformation, with microgels deforming less than the overall sample (Fig. 1d), thus supporting the simulation findings. Given that the microgels were precrosslinked, we hypothesize that phase interactions are predominantly driven by reversible physical interactions, particularly hydrogen bonds. During compression, these hydrogen bonds break, leading to separation between the microgel and the matrix, which is further validated by confocal imaging (Fig. 1d; Fig. S1b in the supplementary information).

3.2 Effects of microgel proportion on the mechanical properties

The mechanical properties and fatigue resistance of hydrogels under compressive loads are essential for biomedical applications such as tissue regeneration scaffolds [30]. We hypothesize that during compression, the GC hydrogel may behave similarly to human adipose tissue, which absorbs pressure for protection (Fig. 2a). To explore this, we investigated how varying the microgel proportion affects the mechanical properties of GC hydrogels, while keeping the properties of the microgels and the interstitial matrix consistent. We prepared GC hydrogels with microgel proportions of 40%, 60%, and 80%, as well as a jammed-microgel hydrogel (100% microgel content) and a bulk hydrogel made entirely from the interstitial matrix (0% microgel). The stress–strain curves (Fig. 2b) indicated that an increase in the microgel proportion gradually reduced the elastic modulus of the GC hydrogel (Fig. 2c), without significantly altering the fracture strain (Fig. 2d); this was likely due to the lower modulus of the microgels. Although jammed microgel bioinks and pure GelMA hydrogels fail rapidly under cyclic compression, the GC hydrogel with 60% microgel content exhibited excellent performance under 60% strain, showing minimal variation in peak stress over 100 cycles (Fig. 2e). However, at 70% strain, rapid fatigue was observed (Figs. 2f and 2g). Notably, a GC hydrogel with 40% microgel content failed quickly during 60% strain cycling (Fig. 2h), demonstrating significantly reduced cyclic performance compared to the 60% microgel sample (Figs. 2i and 2j). These results suggest that varying microgel proportions define distinct elastic limits, establishing the maximum strain at which cyclic performance can be sustained. In addition, we investigated the degradation behavior of GC hydrogels with differing microgel proportions (Fig. S2 in the supplementary information). Our results reveal that an increase in microgel proportion accelerates the degradation rate of GC hydrogels. This may be due to the system's mechanical strength and the topological characteristics of the matrix phase. A higher microgel

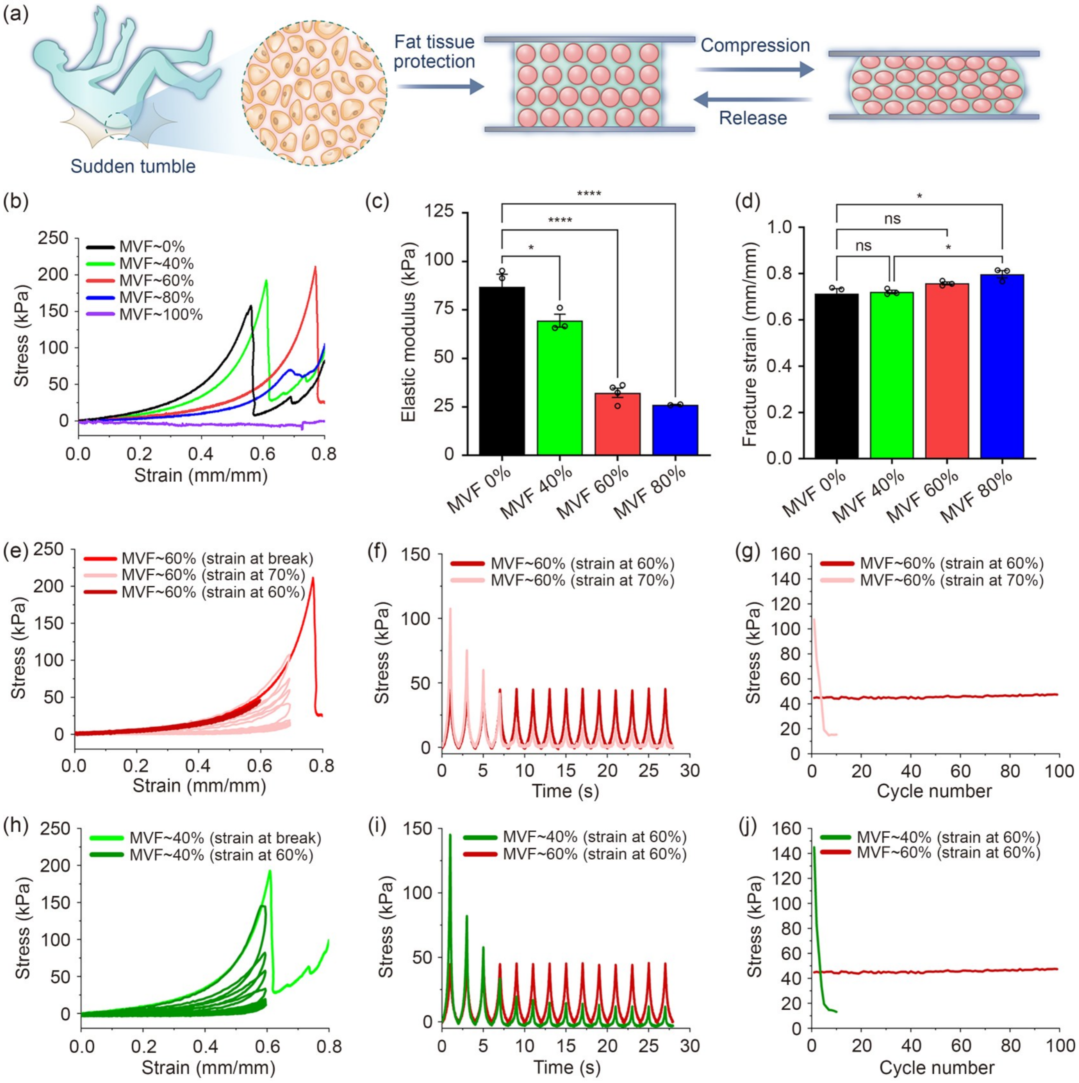

Fig. 2 Effects of microgel proportion on the mechanical properties: (a) schematic of the compression principle for GC hydrogels; (b) compression stress–strain curves for GC hydrogels at various microgel proportions; (c) elastic modulus; (d) fracture strain; (e) cyclic compression stress–strain curves for samples containing 60% microgels; (f) cyclic compression stress–time curves for samples with 60% microgels; (g) cyclic compression stress–cycle count curves for samples with 60% microgels; (h) cyclic compression stress–strain curves for samples with 40% microgels; (i) cyclic compression stress–time curves for samples with 40% and 60% microgels; (j) cyclic compression stress–cycle count curves for samples with 40% and 60% microgels. One-way ANOVA was used for data analysis. Data in (c, d) are expressed as mean±standard deviation (n=3). $^{*}p<0.05$, $^{****}p<0.0001$. ns: not significant. MVF: microgel volume fraction

proportion contributes to an increased specific surface area, promoting faster degradation. These findings have significant implications for the potential application of GC hydrogels in drug delivery systems. To further showcase the versatility of our design, we created a PEGDA-based GC hydrogel, which yielded similar results, including a lower modulus and excellent cyclic performance (Fig. S3 in the supplementary information). We hypothesize that the interconnected topology of the interstitial matrix results in a combination of bending and compression, enhancing deformability and enabling robust cyclic performance under high strain, akin to the bending deformation observed in graphene aerogels [31]. Moreover, we explored the effects of the modulus of microgels and the matrix phase on the mechanical properties of GC hydrogels. We fabricated microgels and matrix phases using GelMA at three different concentrations of soft (3%), medium (7.5%), and stiff (15%), and prepared GC hydrogels with a 60% microgel proportion. We observed that as the matrix concentration remained constant, the modulus of GC hydrogels increased with higher microgel concentrations (Figs. S4a and S4b in the supplementary information), whereas the softer microgels exhibited improved cyclic performance (Fig. S4c in the supplementary information). A similar trend was noted when the microgel concentration was fixed and matrix concentrations varied (Fig. S5 in the supplementary information). This relationship between elastic modulus and concentration aligns with the theoretical predictions outlined in Sect. 2.8. Regarding cyclic performance, we hypothesize that softer GC hydrogel components enable a more uniform distribution and transfer of stress, thereby reducing stress concentrations and the formation of defects. Finally, we fabricated GC hydrogels by combining stiff microgels with a soft matrix and used shorthand notation to represent the concentrations of both phases, where the numerical values indicate their respective concentrations. For instance, "15D3M" signifies a dispersed phase concentration of 15% and a matrix phase concentration of 3%. The 15D3M sample exhibited a higher modulus than 7.5D7.5M while maintaining excellent cyclic performance. Based on these findings, we propose a generalized strategy for tailoring the mechanical properties of GC hydrogels by adjusting the modulus and proportion of their two constituent phases.

3.3 Effects of hydrogen bonds on mechanical properties

Photocrosslinking of GelMA chains creates a covalently crosslinked network in both phases of the GelMA-based GC hydrogel. The aldehyde and amino groups on the GelMA polymer chains enable hydrogen bonding at the phase interface, acting as both donors and acceptors [32]. Considering the precrosslinked nature of the microgels, we hypothesize that reversible physical interactions, particularly hydrogen bonds, affect the mechanical properties of the hydrogel. To test this hypothesis, we selected the GC hydrogel with 60% microgel content to better understand the role of hydrogen bonds in compressive and cyclic properties. Urea, a recognized hydrogen bond disruptor, competes with polymer chains for hydrogen bond sites, thereby disrupting the hydrogen bonding network [33–35]. Following photopolymerization, samples were soaked in a 1.0-mol/L urea solution to achieve full swelling prior to testing, with a control group soaked in PBS for comparison. The results indicated that the elastic modulus of the urea-treated samples (14.46 kPa) was significantly lower than that of the control samples (23.81 kPa) (Fig. 3b). Toughness was also noticeably reduced (Fig. 3c), whereas the fracture strain and stress remained similar between the two groups (Figs. 3d and 3e). The urea-treated and control samples displayed excellent cyclic performance, with the urea-treated sample showing a lower modulus but no significant difference in the ratio of maximum stress after 100 cycles compared to the initial maximum stress (89.18%

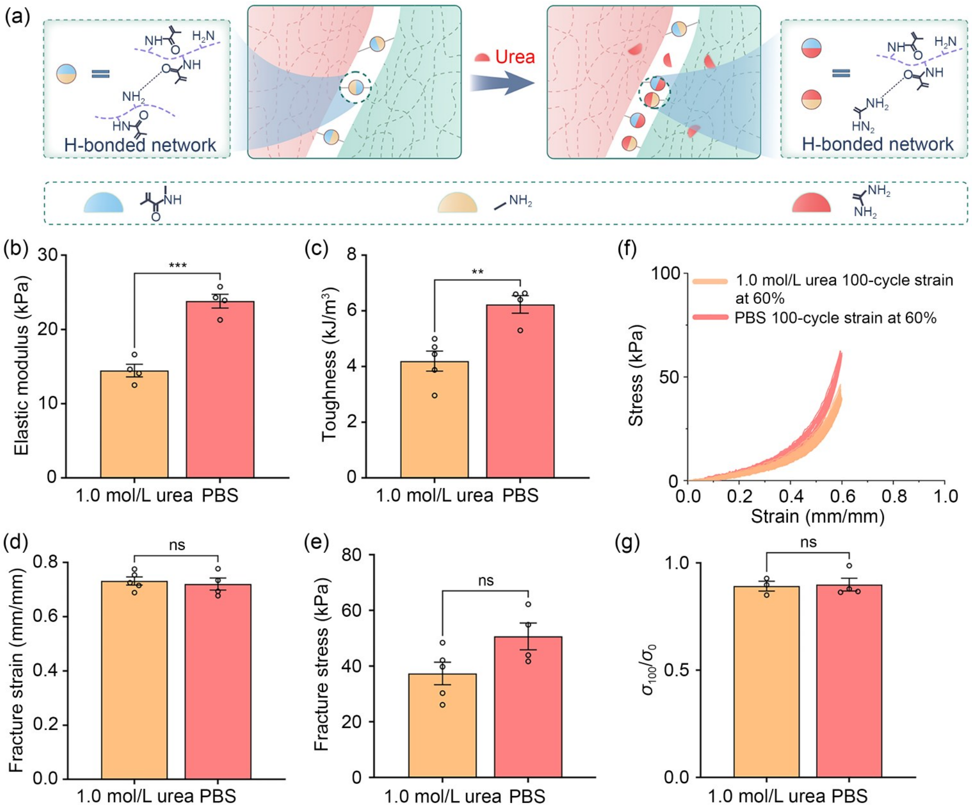

Fig. 3 Effects of hydrogen bonds on mechanical properties: (a) schematic of the hydrogen bond distribution within the GC hydrogel and interfacial hydrogen bonds, along with the mechanism by which urea disrupts hydrogen bonds; (b) elastic modulus (*n*=4); (c) toughness (*n*=5); (d) fracture strain (*n*=5); (e) fracture stress (*n*=5); (f) stress–strain curve during cyclic compression; (g) comparison of the ratio of stress after 100 cycles to the initial stress between the urea-treated samples and the control samples (*n*=5). One-way ANOVA was used for data analysis. Data in (b–e, g) are expressed as mean±standard deviation. $^{**}p<0.01$, $^{***}p<0.001$; ns: not significant

for urea-treated vs. 89.89% for control samples) (Fig. 3g). These findings suggest that, although hydrogen bonds affect the modulus of GC hydrogels, they do not significantly influence cyclic performance. We hypothesize that at lower strains, hydrogen bond interactions at the phase interfaces contribute to the modulus, and urea treatment weakens these interactions, resulting in a reduced elastic modulus. At higher strains, the stretching of GelMA chains, driven by covalent bonds, accounts for the similar fracture stress and strain observed. Toughness, which reflects the work done during compression, is affected by hydrogen bonds and the fracture energy of the polymer chains; urea treatment disrupts hydrogen bonds, thereby reducing toughness by eliminating their contribution to the work done.

3.4 Effects of microgel proportion on rheological properties

Ideally, the ink should have high viscosity in the syringe to prevent cell sedimentation, transition to a low-viscosity state under high shear, during extrusion, to protect the cells, and return to its initial viscosity after extrusion to maintain shape (Fig. 4a). The rheological properties are crucial for assessing the suitability of hydrogels as bioinks for bioprinting. We characterized the rheological properties of GC hydrogel precursors with microgel proportions of 40%, 60%, 80%, and 100% (Fig. 4b). All GC hydrogels exhibited shear-thinning behavior at room temperature. As the microgel proportion increased, the temperature sensitivity decreased, thereby expanding the temperature range suitable for 3D printing. In the case of jammed microgels lacking the interstitial matrix, both the storage modulus G' and loss modulus G'' remained relatively constant with temperature (Fig. 4c). GC hydrogels with varying microgel proportions demonstrated both strain-yielding behavior (Fig. 4d) and self-healing properties (Fig. 4e), with higher microgel content resulting in increased yield stress (Fig. 4f). Initially, yield strain decreased with small amounts of interstitial matrix but increased as the proportion of the matrix grew (Fig. 4g). We hypothesize that, prior to crosslinking, microgels act as

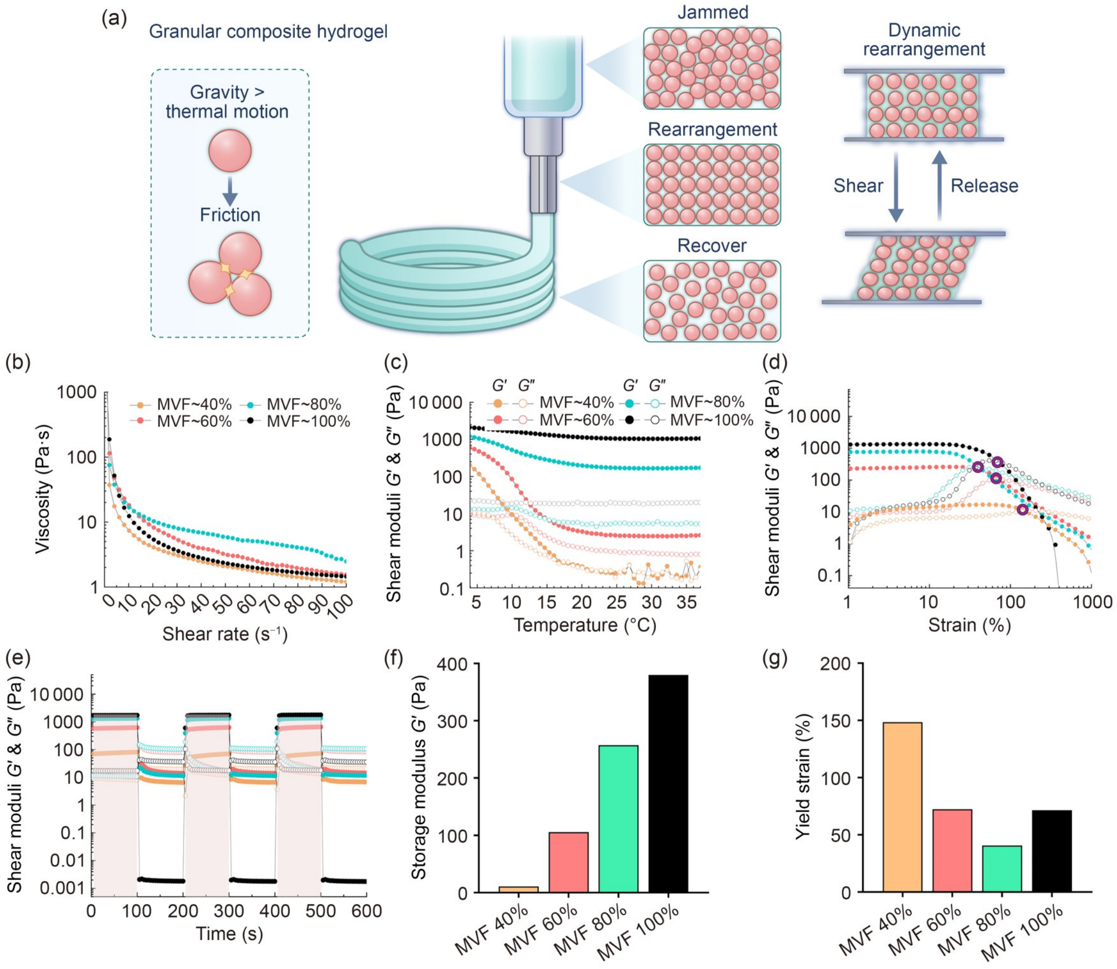

Fig. 4 Effects of microgel proportion on rheological properties: (a) schematic of the printing process for the GC hydrogel; (b) analysis of shear-thinning properties; (c) temperature-sensitive analysis; (d) self-healing behavior under low shear (1%) and high shear (1000%) cycles; (e) strain sweep analysis; (f) yield stress; (g) yield strain. MVF: microgel volume fraction

the solid phase, primarily influencing yield strength, whereas an increased interstitial matrix enhances stress transfer and leads to higher yield strain. We also investigated the effects of microgel size on the rheological and compressive properties of GC hydrogels with 60% microgel content. Microgels with average diameters of 20 μm (batch emulsification, Fig. S7c in the supplementary information) and 200 μm (microfluidic, Fig. S7d in the supplementary information) exhibited shear-thinning behavior (Fig. S8a in the supplementary information) and strain-yielding characteristics (Fig. S8b in the supplementary information). The smaller microgels exhibited lower viscosity, likely due to improved dispersibility and flowability within the matrix. Compression tests indicated no significant differences in elastic modulus between the two microgel sizes (Figs. S8c and S8d in the supplementary information), suggesting that variations at the micron scale do not significantly affect the matrix's crosslinking density or modulus. Larger size differences, such as those between micro- and nanoscale particles, require further investigation. These findings emphasize the tunable rheological properties of GC hydrogels, making them suitable for 3D printing applications.

3.5 3D printing of GC hydrogels for the preoperative planning model

In previous studies, we successfully encapsulated human hepatic and endothelial cells within microgels and the matrix of GC hydrogels to print 3D hepatic tissues, demonstrating improved cell viability and metabolic function compared to GelMA hydrogels [25]. In this study, we extend the application of GC hydrogels to surgical organ models, emphasizing the optimized mechanical and rheological properties of GC hydrogels. By fine-tuning its composition, we achieved an elasticity comparable to human tissue, thus facilitating the creation of 3D-printed models suitable for preoperative surgeon training. We first evaluated the printing performance of GC hydrogels in an AVC-based supporting bath, successfully producing high-fidelity brain, ear, and bronchus models with complex geometries (Figs. 5a–5c). Traditional 3D-printed organ models, typically made from silicone, fail to replicate the liver's elastic modulus and intricate vascular network, which are essential for accurate path planning and anatomical positioning [36–38]. To address this limitation, we utilized SPIRIT printing technology [39] to fabricate a biomimetic

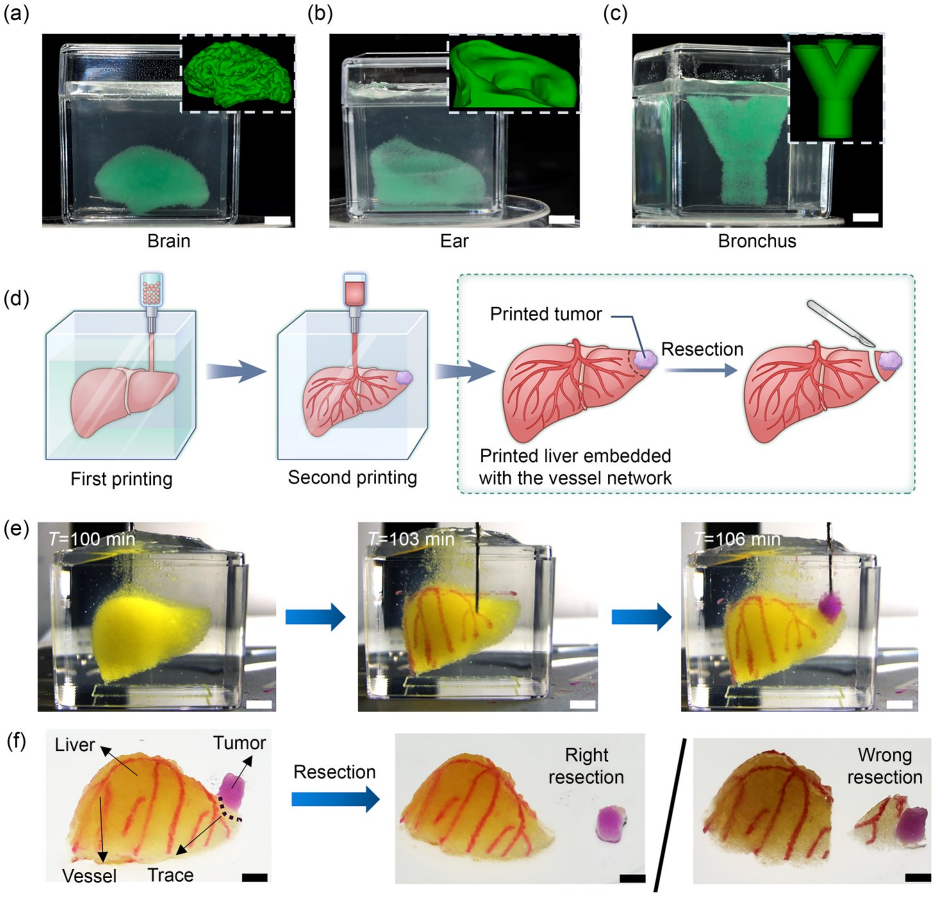

Fig. 5 3D printing of GC hydrogels for the preoperative planning model: (a–c) printing performance of the GC hydrogel (brain, ear, bronchus); (d) scheme of embedded printing and preoperative planning; (e) embedded printing in AVC supporting bath; (f) preoperative planning and resection using a scalpel. Scale bars: 5 mm (a–c), 500 μm (e), and 200 μm (f)

liver model embedded with vascular networks and tumor structures for preoperative planning (Fig. 5d). Specifically, a primary liver model was printed using GC hydrogels in the AVC supporting bath, followed by the sequential printing of the vascular network and tumor structures (Fig. 5e). The success of SPIRIT printing is attributed to the dual-printing capability of GC hydrogels, which serve as both bioink and a temporary supporting bath, enabled by their tunable rheological properties. As Fig. 5f shows, we successfully created a liver model with hierarchical vascular channels and tumor aggregates. Following photopolymerization, the sacrificial template was removed to form the vascular network. Once taken out of the bath, the model was used for preoperative practice, and perfusion experiments confirmed the connectivity of the vascular network (Fig. S9 in the supplementary information). Surgical rehearsals verified the model's utility for tumor resection, enabling the simulation of both correct and incorrect path selections. Moreover, the model demonstrated reusability; following sectioning, GelMA adhesive facilitated light-induced reassembly and repeated resections. This study thus establishes a rational framework for designing GC hydrogels with tailored properties, where the preoperative planning model serves as a proof of concept for their versatile potential in biomedical applications.

4 Conclusions

In this study, we systematically investigated the factors influencing the mechanical properties and printability of GC hydrogels. Using confocal microscopy and nanoindentation, we quantitatively assessed the spatial distribution of microgel interfaces and the variations in modulus. Our results showed that the elastic modulus of GC hydrogels decreased with increasing microgel content while demonstrating improved cyclic properties compared to both jammed microgel and pure GelMA hydrogels. We also discovered that the disruption of hydrogen bonds resulted in reduced modulus and toughness, although it did not affect the fracture or cyclic properties. In addition, we demonstrated the adjustable shear-thinning and self-healing properties of GC hydrogels, which enable the dual-printing capability, functioning as both a printable bioink and a supporting bath for embedded printing. We successfully fabricated a liver model with embedded vascular networks and tumor structures using GC hydrogels, enhancing preoperative training for surgeons. This work establishes a rational framework for the tunable design of GC hydrogels, facilitating their integration into advanced biomedical engineering platforms. In the future, by incorporating bioactive factors or living cells, the tunable mechanical and rheological properties of GC hydrogels can be leveraged to fabricate more complex tissue constructs such as cartilage or breast repair.

Supplementary Information The online version contains supplementary material available at https://doi.org/10.1631/bdm.2500018.

Acknowledgements We gratefully acknowledge the financial support from the National Natural Science Foundation of China (Nos. U21A20394 and 52305314), the Beijing Natural Science Foundation (Nos. 7252285 and L246001), and the National Key Research and Development Program of China (No. 2023YFB4605800). We also extend our sincere thanks to Jianyong Huang (College of Engineering, Peking University) and Qunyang Li (School of Aerospace Engineering, Tsinghua University) for their invaluable insights and stimulating discussions.

Author contributions YCF, TZ, and ZX conceptualized the study and designed this study. HYD, ZXG, and BYW led the design and engineering investigations. HYD and ZXG conducted the experiments and were responsible for data acquisition and analysis. HYD and YCF drafted the manuscript. YCF and ZX supervised and directed the project. YCF, TZ, and ZX secured funding and resources. All authors contributed to the critical revision of the manuscript and approved the final version.

Declarations

Conflict of interest TZ is an associate editor for *Bio-Design and Manufacturing* and was not involved in the editorial review or the decision to publish this article. The authors declare that they have no conflict of interest.

Ethical approval This article does not contain any studies with human or animal subjects performed by any of the authors.

Data availability The data that support the findings of this study are available from the corresponding authors upon reasonable request.

References

1. Nonoyama T, Gong JP (2021) Tough double network hydrogel and its biomedical applications. Annu Rev Chem Biomol Eng 12:393–410. https://doi.org/10.1146/annurev-chembioeng-101220-080338
2. Murphy SV, Atala A (2014) 3D bioprinting of tissues and organs. Nat Biotechnol 32(8):773–785. https://doi.org/10.1038/nbt.2958
3. Yuan XM, Zhu Z, Xia PC et al (2023) Tough gelatin hydrogel for tissue engineering. Adv Sci 10(24):2301665. https://doi.org/10.1002/advs.202301665
4. Wang D, Li QY, Zhou CY et al (2024) Dissolvable temporary barrier: a novel paradigm for flexible hydrogel patterning in organ-on-a-chip models. Bio-Des Manuf 7(2):153–166. https://doi.org/10.1007/s42242-023-00267-x
5. De Nitto S, Serafin A, Karadimou A et al (2024) Development and characterization of 3D-printed electroconductive pHEMA-co-MAA NP-laden hydrogels for tissue engineering. Bio-Des Manuf 7(3):262–276. https://doi.org/10.1007/s42242-024-00272-8
6. Li XY, Gong JP (2024) Design principles for strong and tough hydrogels. Nat Rev Mater 9(6):380–398. https://doi.org/10.1038/s41578-024-00672-3
7. Okumura Y, Ito K (2001) The polyrotaxane gel: a topological gel by figure-of-eight cross-links. Adv Mater 13(7):485–487. https://doi.org/10.1002/1521-4095(200104)13:7<485::AID-ADMA485>3.0.CO;2-T
8. Ito K (2007) Novel cross-linking concept of polymer network:

synthesis, structure, and properties of slide-ring gels with freely movable junctions. Polym J 39(6):489–499. https://doi.org/10.1295/polymj.PJ2006239

9. Noda Y, Hayashi Y, Ito K (2014) From topological gels to slide-ring materials. J Appl Polym Sci 131(15):40509. https://doi.org/10.1002/app.40509
10. Liu C, Kadono H, Mayumi K et al (2017) Unusual fracture behavior of slide-ring gels with movable cross-links. ACS Macro Lett 6(12):1409–1413. https://doi.org/10.1021/acsmacrolett.7b00729
11. Sakai T, Matsunaga T, Yamamoto Y et al (2008) Design and fabrication of a high-strength hydrogel with ideally homogeneous network structure from tetrahedron-like macromonomers. Macromolecules 41(14):5379–5384. https://doi.org/10.1021/ma800476x
12. Kamata H, Akagi Y, Kayasuga-Kariya Y et al (2014) "Non-swellable" hydrogel without mechanical hysteresis. Science 343(6173):873–875. https://doi.org/10.1126/science.1247811
13. Gong JP, Katsuyama Y, Kurokawa T et al (2003) Double-network hydrogels with extremely high mechanical strength. Adv Mater 15(14):1155–1158. https://doi.org/10.1002/adma.200304907
14. Nakajima T, Ozaki Y, Namba R et al (2019) Tough double-network gels and elastomers from the nonprestretched first network. ACS Macro Lett 8(11):1407–1412. https://doi.org/10.1021/acsmacrolett.9b00679
15. Hu XL, He J, Qiao L et al (2024) Multifunctional dual network hydrogel loaded with novel tea polyphenol magnesium nanoparticles accelerates wound repair of MRSA infected diabetes. Adv Funct Mater 34(22):2312140. https://doi.org/10.1002/adfm.202312140
16. Fang YH, Liang C, Liljeström V et al (2024) Toughening hydrogels with fibrillar connected double networks. Adv Mater 36(27): 2402282. https://doi.org/10.1002/adma.202402282
17. Zhang XN, Wang YJ, Sun ST et al (2018) A tough and stiff hydrogel with tunable water content and mechanical properties based on the synergistic effect of hydrogen bonding and hydrophobic interaction. Macromolecules 51(20):8136–8146. https://doi.org/10.1021/acs.macromol.8b01496
18. Wu YQ, Shi YQ, Wang HL (2023) Urea as a hydrogen bond producer for fabricating mechanically very strong hydrogels. Macromolecules 56(12):4491–4502. https://doi.org/10.1021/acs.macromol.3c00611
19. Li P, Zhao J, Chen Y et al (2017) Preparation and characterization of chitosan physical hydrogels with enhanced mechanical and antibacterial properties. Carbohyd Polym 157:1383–1392. https://doi.org/10.1016/j.carbpol.2016.11.016
20. Liu XY, He X, Yang B et al (2021) Dual physically cross-linked hydrogels incorporating hydrophobic interactions with promising repairability and ultrahigh elongation. Adv Funct Mater 31(3): 2008187. https://doi.org/10.1002/adfm.202008187
21. Nonoyama T, Lee YW, Ota K et al (2020) Instant thermal switching from soft hydrogel to rigid plastics inspired by thermophile proteins. Adv Mater 32(4):1905878. https://doi.org/10.1002/adma.201905878
22. Shin M, Song KH, Burrell JC et al (2019) Injectable and conductive granular hydrogels for 3D printing and electroactive tissue support. Adv Sci 6(20):1901229. https://doi.org/10.1002/advs.201901229
23. Highley CB, Song KH, Daly AC et al (2019) Jammed microgel inks for 3D printing applications. Adv Sci 6(1):1801076. https://doi.org/10.1002/advs.201801076
24. Daly AC, Riley L, Segura T et al (2020) Hydrogel microparticles for biomedical applications. Nat Rev Mater 5(1):20–43. https://doi.org/10.1038/s41578-019-0148-6
25. Fang YC, Guo YH, Ji MK et al (2022) 3D printing of cell-laden microgel-based biphasic bioink with heterogeneous microenvironment for biomedical applications. Adv Funct Mater 32(13): 2109810. https://doi.org/10.1002/adfm.202109810
26. Fang YC, Ji MK, Wu BY et al (2023) Engineering highly vascularized bone tissues by 3D bioprinting of granular prevascularized spheroids. ACS Appl Mater Interfaces 15(37):43492–43502. https://doi.org/10.1021/acsami.3c08550
27. Deo KA, Murali A, Tronolone JJ et al (2024) Granular biphasic colloidal hydrogels for 3D bioprinting. Adv Healthc Mater 13(25): 2303810. https://doi.org/10.1002/adhm.202303810
28. William DC, David GR (2018) Materials Science and Engineering: An Introduction (10th Ed.). Wiley, USA
29. He J, Sun Y, Gao Q et al (2023) Gelatin methacryloyl hydrogel, from standardization, performance, to biomedical application. Adv Healthc Mater 12(23):2300395. https://doi.org/10.1002/adhm.202300395
30. Zhang T, Jin L, Fang YC et al (2014) Fabrication of biomimetic scaffolds with oriented porous morphology for cardiac tissue engineering. J Biomater Tiss Eng 4(12):1030–1039. https://doi.org/10.1166/jbt.2014.1255
31. Wu MM, Geng HY, Hu YJ et al (2022) Superelastic graphene aerogel-based metamaterials. Nat Commun 13(1):4561. https://doi.org/10.1038/s41467-022-32200-8
32. Liu BC, Wang Y, Miao Y et al (2018) Hydrogen bonds autonomously powered gelatin methacrylate hydrogels with super-elasticity, self-heal and underwater self-adhesion for sutureless skin and stomach surgery and E-skin. Biomaterials 171:83–96. https://doi.org/10.1016/j.biomaterials.2018.04.023
33. Zhang XY, Zhao CZ, Xiang NP et al (2016) Chain entanglements and hydrogen bonds in carbopol microgel reinforced hydrogel. Macromol Chem Phys 217(19):2139–2144. https://doi.org/10.1002/macp.201600245
34. Dai XY, Zhang YY, Gao LN et al (2015) A mechanically strong, highly stable, thermoplastic, and self-healable supramolecular polymer hydrogel. Adv Mater 27(23):3566–3571. https://doi.org/10.1002/adma.201500534
35. Huang Y, Zhong M, Huang Y et al (2015) A self-healable and highly stretchable supercapacitor based on a dual crosslinked polyelectrolyte. Nat Commun 6:10310. https://doi.org/10.1038/ncomms10310
36. Dong JH, Yang SZ, Zeng JP et al (2013) Precision in liver surgery. Semin Liver Dis 33(3):189–203. https://doi.org/10.1055/s-0033-1351781
37. Fang CH, Zhang P, Qi XL (2019) Digital and intelligent liver surgery in the new era: prospects and dilemmas. EBioMedicine 41:693–701. https://doi.org/10.1016/j.ebiom.2019.02.017
38. Lu YH, Chen X, Han F et al (2023) 3D printing of self-healing personalized liver models for surgical training and preoperative planning. Nat Commun 14(1):8447. https://doi.org/10.1038/s41467-023-44324-6
39. Fang YC, Guo YH, Wu BY et al (2023) Expanding embedded 3D bioprinting capability for engineering complex organs with freeform vascular networks. Adv Mater 35(22):2205082. https://doi.org/10.1002/adma.202205082